

Tabular Electrical Conductivity for Aluminum

C. E. Starrett,^{1,*} R. Perriot,¹ N. R. Shaffer,¹ T. Nelson,¹ L. A. Collins,¹ and C. Ticknor¹

¹*Los Alamos National Laboratory, P.O. Box 1663, Los Alamos, NM 87545, U.S.A.*

(Dated: November 18, 2019)

A new Sesame-type table for the electrical conductivity of aluminum is described. The table is based on density functional theory calculations and ranges from 10^{-3} to 1 times solid density (2.7 g/cm^3), and from 10^{-2} to 10^3 eV in temperature. The table is compared to other simulations and to experiments and is generally in good agreement. The high temperature, classical limit of the conductivity is recovered for the highest temperatures and lowest densities. The table is critically evaluated and directions for improvements are discussed.

Keywords: electrical conductivity

I. INTRODUCTION

Electrical conductivity in dense materials is an important physical parameter for a variety of applications. For example, it is needed for modelling magnetic liner fusion experiments [1] and pulse power experiments [2], or the dynamo effect in the core of planets [3].

In the low density, high temperature regime, classical methods using Coulomb Logarithms are accurate [4–6] and quick to evaluate. However, in the dense regime these approaches break down due to effects like ion correlation, partial ionization, core-valence orthogonality, degeneracy, and multiple scattering effects [7].

An alternative approach is to use accurate models, that are too expensive and complicated to be used directly in applications, to make data tables. For example, Rinker [8] made Sesame [9] data tables based on an average atom approach coupled to the Ziman approximation [10]. This method is reasonable in the degenerate regime (high density, low temperature), but is inaccurate elsewhere. Desjarlais [11] also made Sesame tables by adjusting the Coulomb Log based Lee-More model [5] to better match available experimental data among other improvements. Another approach is to use a chemical-model [12], which can be rapid to evaluate but does not include some relevant physics like ionic structure (for a review see reference [13]).

We take the approach of using high fidelity density functional theory (DFT) based calculations to model the entire density-temperature plane of interest where the material is a fluid. We focus on aluminum, as it is a widely used conductor, but the approach can be applied to other materials. We employ two methods: the accurate but expensive density functional theory molecular dynamics (DFT-MD), coupled to the Kubo-Greenwood approximation [14], which is practical for degenerate systems, and the more approximate Potential of Mean Force approach [15], which is accurate for moderate to weakly degenerate plasmas and is relatively inexpensive.

It is also possible to use the Kubo-Greenwood method

with the average atom model [16–21], but we have opted not to use this approach as it remains to be proven that this contains the correct limiting behaviour at high temperature, and is more computationally expensive. In contrast, the potential of mean force approach which relies on the relaxation time approximation does recover the classical limit [22] and is rapid to evaluate.

II. CONSTRUCTION OF TABLE

The table ranges from 10^{-3} to 1 times solid density, taken here as 2.7 g/cm^3 , and from 10^{-2} to 10^3 eV in temperature. We start by calculating the electrical conductivity for the full range of the table using the potential of mean force model of reference [15]. This model uses the BGK [23] approximation (also known as the relaxation time approximation). The electron relaxation time is calculated using the quantum mechanical expression for the momentum transport cross section

$$\sigma_{\text{tr}}(\epsilon) = \frac{4\pi\hbar^2}{p^2} \sum_{l=0}^{\infty} (l+1) (\sin(\eta_{l+1} - \eta_l))^2 \quad (1)$$

where p is the electron momentum, the η_l are energy dependent phase shifts and the sum over angular momentum quantum number l converges. The phase shifts are evaluated by solving the Schrödinger equation for the scattering potential. This potential, the potential of mean force $V^{MF}(r)$, is calculated using the finite temperature DFT based average atom-two component plasma model (AA-TCP) developed in references [24, 25]. The potential of mean force recovers the Debye-Huckel potential at high temperature and low density. It takes into account core states, core-valence orthogonality, ionic structure (through the pair distribution function), and partial ionization.

This approach to the conductivity becomes inaccurate in systems where the density of states of scattering electrons deviates strongly from free-electron like behaviour. For example, in the expanded metal regime, with temperatures of $\sim 1 \text{ eV}$, and densities $\sim 1/10^{\text{th}}$ of solid (i.e. warm dense matter), where electron states are relocalizing as density is reduced, this model will be inaccurate

*Electronic address: starrett@lanl.gov

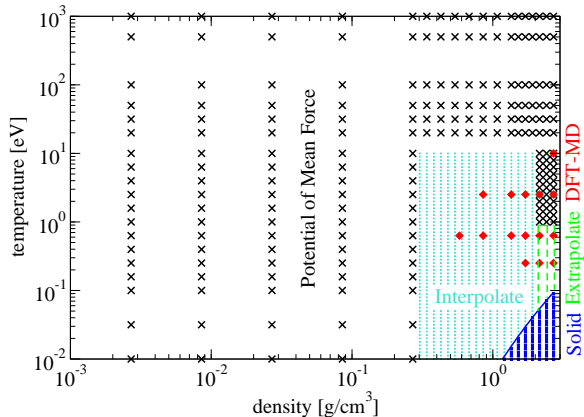


FIG. 1: (Color online) Graphic describing the construction of the table. Black \times 's are density-temperature ($\rho - T$) points for which the potential of mean force model V^{MF} [15] was evaluated. Red diamonds are $\rho - T$ points where we evaluated DFT-MD. The dark blue region in the bottom right hand corner is where the solid model is used. The light blue and green regions correspond to regions of interpolation [28] and extrapolation which were guided by the DFT-MD and V^{MF} results.

(see [15]). In general, however, this model is reasonably accurate and computationally inexpensive, allowing construction of wide ranging tables. Since this is a DFT-based model we must choose an exchange and correlation potential. We have used the temperature dependent LDA parameterization of reference [26]. For the electron-electron contribution to the electrical conductivity we have used the formula given in reference [27].

As a more accurate approach in the warm dense matter regime, we employ quantum molecular dynamics (QMD) in the Born-Oppenheimer approximation, which decouples the ionic from the electronic components. The ions move according to classical equations of motion governed by forces due to the ions and electrons. The electrons receive a quantum mechanical treatment based on temperature-dependent density functional theory (TD-DFT)[31]. We follow the Kohn-Sham (KS) implementation and solve for the electronic orbitals over a set of atoms in a periodically-replicated cell; these orbitals in turn determine the electrical conductivity through the Kubo-Greenwood (KG) approximation [32].

We have performed DFT-MD calculations with the Vienna ab-initio simulation package (VASP [33–36]), using the Generalized Gradient Approximation in the Perdew, Burke, Ernzerhof formulation for the exchange-correlation (XC) functional (GGA-PBE) [29, 37] and a GW three-electron (3e) plane augmented wave (PAW) pseudopotential (PP) [38, 39] with a plane-wave cut-off energy of 750 eV. All of the DFT-MD simulations

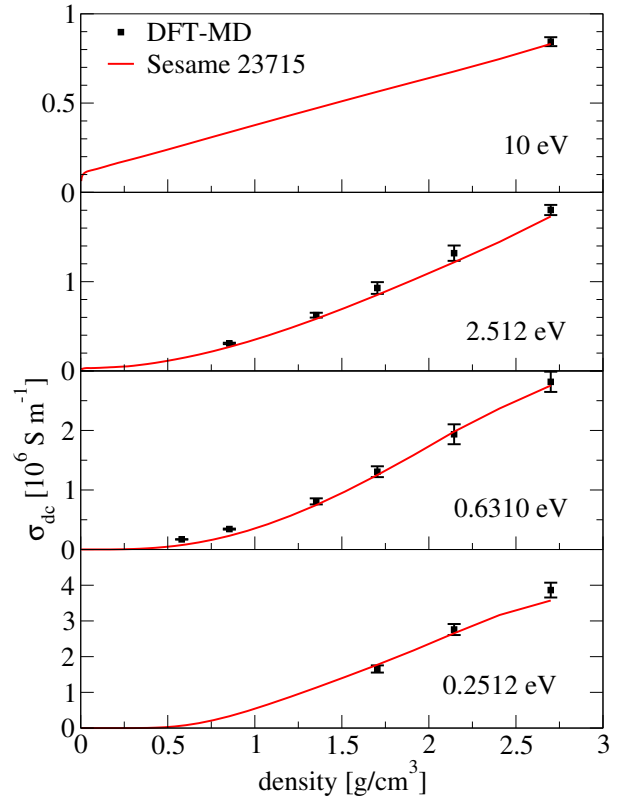


FIG. 2: (Color online) Comparison of new table to DFT-MD results using PBE [29].

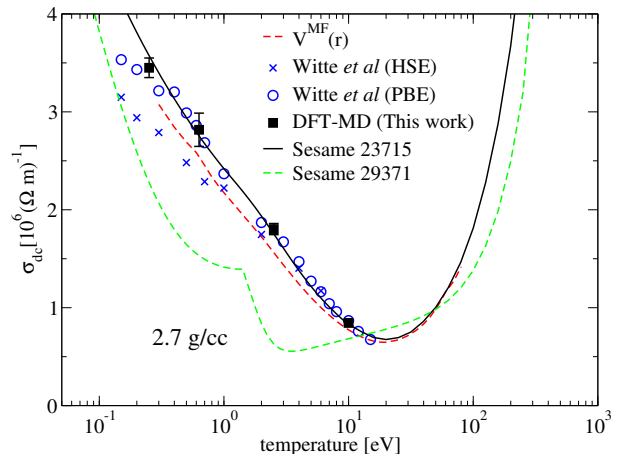


FIG. 3: (Color online) Isochore (2.7 g/cm^3) comparing the new table DFT-MD (this work), Sesame 29371 [11], DFT-MD due to Witte et al [30], and the model of reference [15] ($V^{MF}(r)$).

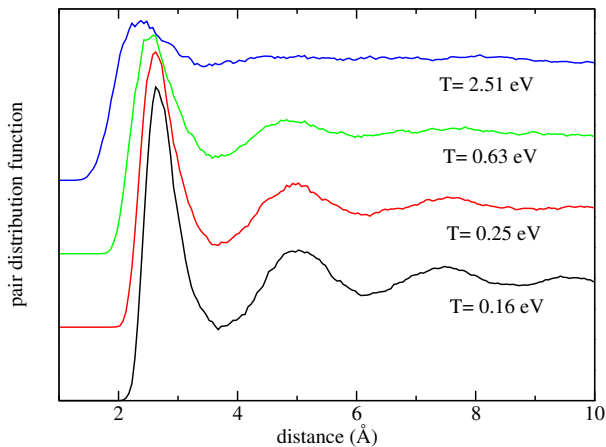


FIG. 4: (Color online) DFT-MD pair distribution functions along an isochore (2.7 g/cm^3). The curves are shifted arbitrarily along the vertical axis for clarity. At the lowest temperatures the pair distribution function displays significant long range structure.

were performed at constant temperature using the Nose-Hoover thermostat with a time step of 1-2 fs at a single k-point (Gamma), containing all orbitals or bands with Fermi-Dirac occupation greater than 1×10^{-4} .

Samples containing 64 atoms at density ρ were first equilibrated at temperature T for at least 2 ps. From this trajectory, we extracted five to ten snapshots separated by a time interval of roughly 2τ in order to determine the frequency-dependent (ac) electrical conductivity by the KG analysis for temperatures between 0.25eV and 10eV. Snapshots separated by the characteristic or e-folding time τ for the velocity autocorrelation function of the self-diffusion coefficient are generally considered uncorrelated ($\tau \approx 20\text{-}140$ ps depending on the density and temperature). For the optical analysis, we employed the Gamma-point or a $2 \times 2 \times 2$ Monkhorst-Pack (MP) grid with four irreducible k-points with the number of bands from twice to three times the MD choice (set I). We have also tested convergence using a $4 \times 4 \times 4$ MP grid with 32 k-points, a GW 11e PAW, and a samples of 128 and 250 atoms (set II). We find for temperatures above 0.5eV, the canonical choice of 64 atoms, GGA-PBE XC functional, GW 3e PAW, and 4 k-points produces results converged within a few percent those of set II for the dc conductivities. For temperatures below 0.5eV, we employ set II although set I gives conductivities within 10%.

We use this method as a benchmark and adjust the table to fit these calculations. Figure 1 shows the points calculated by these models. Most of the temperature-density plane is covered by the potential of mean force model. In the warm dense matter regime the DFT-MD results are used to guide the interpolation and extrapolation regimes where the V^{MF} model is less accurate. Figure 2 shows the comparison of the new table (Sesame 23715) to our DFT-MD calculations. By construction,

the agreement is very good.

In figure 3, we examine the 2.7 g/cm^3 isochore, which displays the new table (Sesame 23715), our DFT-MD calculations, DFT-MD calculations of Witte et al. [30] using two different exchange-correlation potentials (PBE [40] and HSE [41]). Our PBE results agree with those of Witte et al. [30] over the entire temperature range. We also find the need to employ larger k-point and atom samples to obtain converged results below about 0.5eV. This requirement could arise from several conditions, for example, the advent of chemical processes that require more subtle representations of the medium and reactions or the proximity to melt ($\approx 1000\text{K}$). Simulations around melt are notably difficult to perform with methods such as DFT; also, the external constraint applied by the periodic boundary conditions on a small cell can lead to artificial effects, such that representing a disordered (liquid) system under these conditions becomes nontrivial. For example, we show in Fig. 4 by means of the radial distribution function at $\rho=2.7 \text{ g/cm}^3$, the increase in structural features in the form of nearest-neighbor peaks as the temperature decreases.

The potential of mean force results (V^{MF}) are also in reasonable agreement with the DFT-MD (figure 3), and the agreement improves as temperature increases. The new table (by design) matches the DFT-MD using PBE at the lower temperatures and the V^{MF} results at high temperatures. Also shown is the older Sesame 29371 based on the model [5, 11]. Some significant differences between the Tables are observed ($> 50\%$) that could be important in applications (e.g. [42]).

In figure 5, we compare the new table to the experiments of DeSilva et al [43] and Cl erouin et al [44]. These experiments test the difficult expanded metal regime at relatively low temperature, and test our interpolation regime (figure 1), where we have used Akima interpolation [28]. The agreement is reasonable, given that there is a significant discrepancy between the experiments themselves, and with the DFT-MD of reference [14]. The results of the V^{MF} model (not shown, but identical to the new table for densities $< 0.27 \text{ g/cm}^3$) are sensitive to the choice of exchange and correlation potential in this regime. Here we have used the temperature dependent LDA [26]. In reference [15] we used a zero temperature parameterization [47], and found better agreement with the DFT-MD (which also used a zero temperature parameterization). The reason for this sensitivity is the low ionization of the system, and hence the small number of conducting electrons. A small absolute change in this number caused by changing the exchange and correlation potential is a significant relative change, hence the effect on the conductivity. We have chosen to use the more physically complete temperature dependent exchange and correlation potential [26]. Also shown in the figure is the older Sesame 29371 table. It agrees well with the DeSilva et al data by construction but deviates from the DFT-MD at higher densities.

The new table is compared to experiments in the liquid

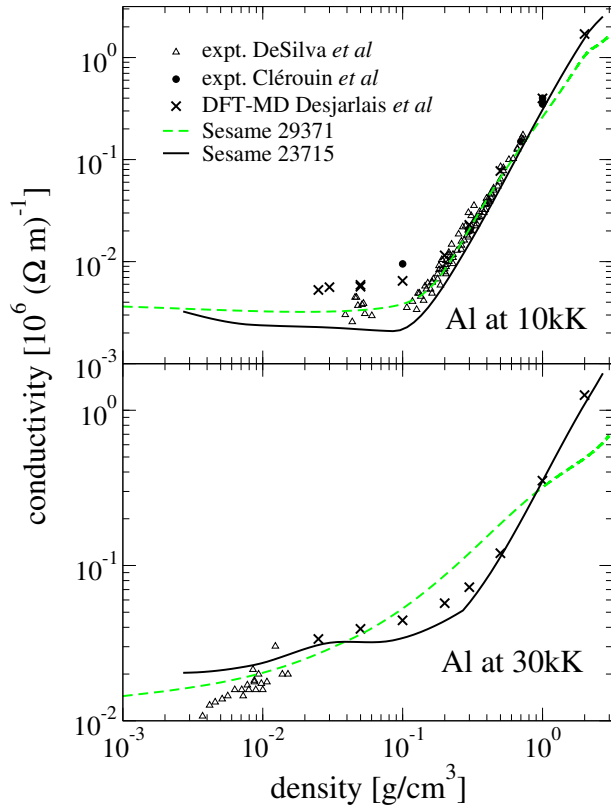


FIG. 5: (Color online) Isotherms (10 kK \approx 0.86 eV, 30 kK \approx 2.59 eV) for expanded aluminum compared to the experiments of DeSilva *et al* [43], experiment of Clérrouin *et al* [44], and DFT-MD of Desjarlais [14].

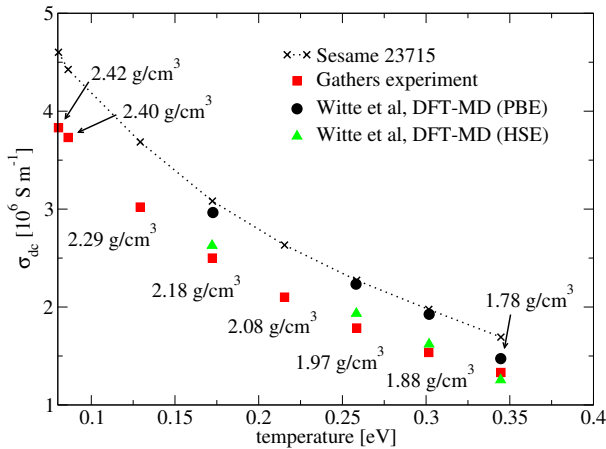


FIG. 6: (Color online) Comparison to the experiments of Gathers [45]. These data have recently been confirmed by another experiment [46]. Also show are DFT-MD results of Witte *et al* [30]. The line connecting the Sesame 23715 points serves only as a guide to the eye.

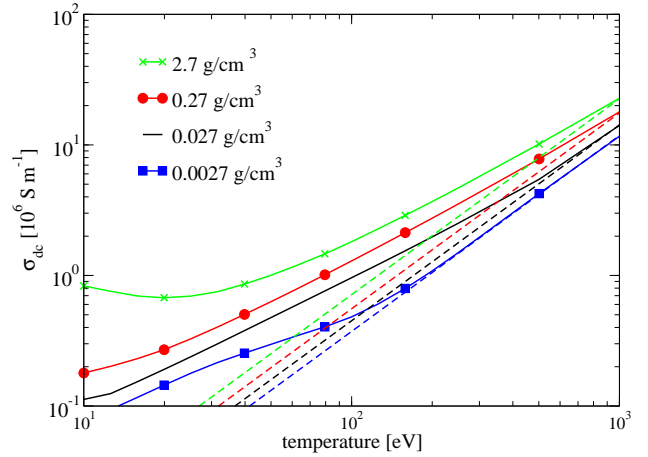


FIG. 7: (Color online) Asymptotic behavior of the new table. The dashed lines have slope $T^{3/2}$ (which is correct in the classical limit), and are fitted to match the table at 1000 eV. At the lowest density and highest temperatures the table recovers this slope.

regime in figure 6. These data have recently been confirmed in reference [46]. Also shown are DFT-MD results from reference [30]. The new table agrees well with the PBE calculations, as expected since it was constructed to match our own PBE calculations in this regime (but not these exact points). The table and the PBE results overestimate the data. HSE calculations by the same authors [30] demonstrate sensitivity to the exchange and correlation potential in this regime.

At high temperatures and low densities the conductivity should be well described by the Spitzer model [4] where the conductivity increases proportionally to $T^{3/2}$ along an isochore. In figure 7 isochores from the table are shown. At the lowest density (10^{-3} times solid density), the model clearly reaches this classical result. This behaviour is not enforced, but rather is a consequence of the BGK model coupled to the quantum cross section (equation (1)) going over to its classical limit. From the figure, as density is increased, this classical behaviour is reached at increasingly high temperature, and for the two highest densities the classical behaviour is not reached by 1000 eV.

In the solid regime (figure 1) we have used the same model as given in reference [5]. The adjustable parameter in that model is tuned to match the data given in reference [49]. The melt line is tuned to fit the experiment of reference [46]. Note that no special consideration is given to the solidus-liquidus region, or to the liquid-vapour coexistence region. The model of reference [5] is simply used below T_{melt} , and above T_{melt} the DFT based model is used. In figure 8 we show a comparison of the new table to the experiments of reference [46, 48]. To avoid interpolation artifacts we have shown the two isochores

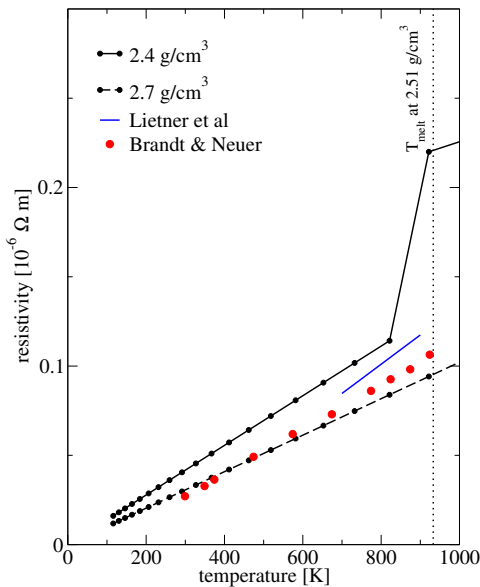


FIG. 8: (Color online) Solid aluminum resistivity. Shown are experimental points due to [48] and a recent set of measurements due to Leitner et al [46], where we have shown the fit given in their paper and the density runs from 2.53 to 2.63 g/cm^3 for the line shown. Two adjacent isochores from the new table are shown (2.7 and 2.4 g/cm^3) that should, if the table is accurate, bracket the experimental data. Note that other experimental data from refs. [49–51] are in close agreement with the Brandt and Neuer data.

that should bracket the data (which account for thermal expansion). Recall that the solid model was tuned to match the Desai data at melt [49], and the Desai data are in agreement with the Brandt data [48]. The new table does bracket the data for $T > 500$ K, but below this there is a small disagreement. The fault likely lies with the relatively crude solid model that we have used. Note that Leitner et al comment in their paper [46] that their data in the solid phase should be regarded as an estimate. The liquid phase data are thought to be accurate (figure 6).

III. DISCUSSION

The new table recovers the known limit at high temperature and agrees reasonable well with the limited experimental data available. Though it interpolates (using

Akima interpolation [28]) through the low temperature expanded metal regime, this interpolation was guided by DFT-MD calculations and as a result is reasonable in this regime. The table is based on DFT calculations that have no adjustable parameters. However, the choice of exchange and correlation potential is clearly important in the low temperature regime (at high temperatures the results are insensitive to this choice). It seems likely that our DFT-MD results would be made more accurate by using the HSE functional, though this is much more computationally expensive and we are already pushing the limits of what is practical for table production.

The simple model that we have used for the solid phase could be improved but such an effort would only be warranted if lower temperatures (i.e. below 10^{-2} eV ≈ 116 K) or higher accuracy are needed. Further, we have given no special consideration to the solidus-liquidus region, or to the coexistence region. This could be improved, but is difficult in practice due to the finite size limitations of the DFT approach.

IV. CONCLUSIONS

A new Sesame-type table for the electrical conductivity of aluminum has been presented. The table is constructed from density-functional theory based calculations. Comparisons to experiments in the solid, liquid and plasma regimes show good agreement. The high temperature, classical limit is recovered. Avenues for improvement have been discussed. The table should be useful for users in the dense plasma community.

Acknowledgments

Los Alamos National Laboratory is operated by Triad National Security, LLC, for the National Nuclear Security Administration of U.S. Department of Energy (Contract No. 89233218NCA000001). We wish to acknowledge useful conversations with Dr. Suxing Hu.

Appendix A: DFT-MD results

The results for the electrical conductivity from our Kubo-Greenwood, DFT-MD simulations are given in table I.

[1] Matthew R. Gomez, Stephen A. Slutz, Adam B. Sefkow, Daniel B. Sinars, Kelly D. Hahn, Stephanie B. Hansen, Eric C. Harding, Patrick F. Knapp, Paul F. Schmit, Christopher A. Jennings, et al. Experimental demonstration of fusion-relevant conditions in magnetized liner inertial fusion. *Physical review letters*, 113(15):155003,

2014.

[2] W.A. Stygar, T.J. Awe, J.E. Bailey, N.L. Bennett, E.W. Breden, E.M. Campbell, R.E. Clark, R.A. Cooper, M.E. Cuneo, J.B. Ennis, et al. Conceptual designs of two petawatt-class pulsed-power accelerators for high-energy-density-physics experiments. *Physical Review Special*

TABLE I: DFT-MD results in units of 10^6 S m^{-1} . The value is obtained from averaging the conductivity over 10 snapshots, and the error corresponds to the standard deviation over the 10 measurements. Cases with low density and/or high temperature require up to several thousands of bands for the MD alone, and were excluded due to the high computational cost. Cases with low temperature and low density resulted in solid-like configurations, and were also excluded.

| | | Density [g/cm^3] | | | | | |
|------------------|-------|-----------------------------|-------------------|-------------------|-------------------|-------------------|-------------------|
| | | 0.539 | 0.854 | 1.353 | 1.704 | 2.145 | 2.700 |
| Temperature [eV] | 10.0 | | | | | | 0.844 ± 0.025 |
| | 2.51 | | 0.308 ± 0.008 | 0.625 ± 0.027 | 0.929 ± 0.066 | 1.319 ± 0.086 | 1.803 ± 0.057 |
| | 0.631 | 0.170 ± 0.003 | 0.342 ± 0.009 | 0.809 ± 0.051 | 1.307 ± 0.091 | 1.936 ± 0.167 | 2.817 ± 0.170 |
| | 0.251 | | | 1.654 ± 0.101 | 2.759 ± 0.155 | 3.45 ± 0.1 | |

- Topics-Accelerators and Beams*, 18(11):110401, 2015.
- [3] Frank D. Stacey and Orson L. Anderson. Electrical and thermal conductivities of feni alloy under core conditions. *Physics of the Earth and Planetary Interiors*, 124(3):153 – 162, 2001.
- [4] Robert S. Cohen, Lyman Spitzer, and Paul McR. Routly. The electrical conductivity of an ionized gas. *Phys. Rev.*, 80:230–238, Oct 1950.
- [5] Yim T. Lee and R. M. More. An electron conductivity model for dense plasmas. *The Physics of fluids*, 27(5):1273–1286, 1984.
- [6] S.I. Braginskii. Transport phenomena in a completely ionized two-temperature plasma. *Sov. Phys. JETP*, 6(33):358–369, 1958.
- [7] C. E. Starrett. Coulomb log for conductivity of dense plasmas. *Physics of Plasmas*, 25(9):092707, 2018.
- [8] George A. Rinker. Systematic calculations of plasma transport coefficients for the periodic table. *Phys. Rev. A*, 37:1284–1297, 1988.
- [9] Stanford P. Lyon. Sesame: the Los Alamos National Laboratory equation of state database. *Los Alamos National Laboratory report LA-UR-92-3407*, 1992.
- [10] John M Ziman. *Electrons and phonons: the theory of transport phenomena in solids*. Oxford University Press, 1960.
- [11] M.P. Desjarlais. Practical improvements to the lee-more conductivity near the metal-insulator transition. *Contributions to Plasma Physics*, 41(2-3):267–270, 2001.
- [12] S. Kuhlbrodt, B. Holst, and R. Redmer. COMPTRA04 a program package to calculate composition and transport coefficients in dense plasmas. *Contributions to Plasma Physics*, 45(2):73–88, 2005.
- [13] Ronald Redmer. Physical properties of dense, low-temperature plasmas. *Physics Reports*, 282(2):35 – 157, 1997.
- [14] M. P. Desjarlais, J. D. Kress, and L. A. Collins. Electrical conductivity for warm, dense aluminum plasmas and liquids. *Phys. Rev. E*, 66:025401, Aug 2002.
- [15] C.E. Starrett. Potential of mean force for electrical conductivity of dense plasmas. *High Energy Density Physics*, 25:8 – 14, 2017.
- [16] C. E. Starrett, J Cl rouin, V Recoules, J. D. Kress, L. A. Collins, and D. E. Hanson. Average atom transport properties for pure and mixed species in the hot and warm dense matter regimes. *Physics of Plasmas (1994-present)*, 19(10):102709, 2012.
- [17] N.M. Gill and C.E. Starrett. Mean-force scattering potential for calculating optical properties of dense plasmas. *High Energy Density Physics*, 31:24 – 30, 2019.
- [18] G. Faussurier, C. Blancard, P. Combis, and L. Videau. Electrical and thermal conductivities in dense plasmas. *Physics of Plasmas (1994-present)*, 21(9):092706, 2014.
- [19] A.A. Ovechkin, P.A. Loboda, and A.L. Falkov. Transport and dielectric properties of dense ionized matter from the average-atom reseoos model. *High Energy Density Physics*, 20:38 – 54, 2016.
- [20] P.A. Sterne, S.B. Hansen, B.G. Wilson, and W.A. Isaacs. Equation of state, occupation probabilities and conductivities in the average atom purgatorio code. *High Energy Density Physics*, 3(12):278 – 282, 2007. Radiative Properties of Hot Dense Matter.
- [21] W.R. Johnson, C. Guet, and G.F. Bertsch. Optical properties of plasmas based on an average-atom model. *Journal of Quantitative Spectroscopy and Radiative Transfer*, 99(13):327 – 340, 2006. Radiative Properties of Hot Dense Matter.
- [22] C. E. Starrett. High-temperature electronic structure with the Korringa-Kohn-Rostoker green’s function method. *Phys. Rev. E*, 97:053205, May 2018.
- [23] P. L. Bhatnagar, E. P. Gross, and M. Krook. A model for collision processes in gases. i. Small amplitude processes in charged and neutral one-component systems. *Phys. Rev.*, 94:511–525, May 1954.
- [24] C. E. Starrett and D. Saumon. Electronic and ionic structures of warm and hot dense matter. *Phys. Rev. E*, 87:013104, Jan 2013.
- [25] C.E. Starrett and D. Saumon. A simple method for determining the ionic structure of warm dense matter. *High Energy Density Physics*, 10:35 – 42, 2014.
- [26] Valentin V. Karasiev, Travis Sjostrom, James Dufty, and S. B. Trickey. Accurate homogeneous electron gas exchange-correlation free energy for local spin-density calculations. *Phys. Rev. Lett.*, 112:076403, Feb 2014.
- [27] H. Reinholz, G. R pke, S. Rosmej, and R. Redmer.

- Conductivity of warm dense matter including electron-electron collisions. *Physical Review E*, 91(4):043105, 2015.
- [28] Hiroshi Akima. A new method of interpolation and smooth curve fitting based on local procedures. *Journal of the ACM (JACM)*, 17(4):589–602, 1970.
- [29] John P. Perdew, Kieron Burke, and Matthias Ernzerhof. Generalized gradient approximation made simple. *Physical review letters*, 77(18):3865, 1996.
- [30] B. B. L. Witte, P. Sperling, M. French, V. Recoules, S. H. Glenzer, and R. Redmer. Observations of non-linear plasmon damping in dense plasmas. *Physics of Plasmas*, 25(5):056901, 2018.
- [31] R.L. Martin. *Electronic Structure*. Cambridge University Press, 2004.
- [32] D.A. Greenwood. The boltzmann equation in the theory of electrical conduction in metals. *Proceedings of the Physical Society*, 71(4):585, 1958.
- [33] Georg Kresse and Jürgen Hafner. Ab initio molecular dynamics for liquid metals. *Physical Review B*, 47(1):558, 1993.
- [34] Georg Kresse and Jürgen Hafner. Ab initio molecular-dynamics simulation of the liquid-metal–amorphous-semiconductor transition in germanium. *Physical Review B*, 49(20):14251, 1994.
- [35] Georg Kresse and Jürgen Furthmüller. Efficiency of ab-initio total energy calculations for metals and semiconductors using a plane-wave basis set. *Computational materials science*, 6(1):15–50, 1996.
- [36] Georg Kresse and Jürgen Furthmüller. Efficient iterative schemes for ab initio total-energy calculations using a plane-wave basis set. *Physical review B*, 54(16):11169, 1996.
- [37] John P. Perdew, Kieron Burke, and Matthias Ernzerhof. Generalized gradient approximation made simple [phys. rev. lett. 77, 3865 (1996)]. *Phys. Rev. Lett.*, 78:1396–1396, Feb 1997.
- [38] Peter E Blöchl. Projector augmented-wave method. *Physical review B*, 50(24):17953, 1994.
- [39] Georg Kresse and D Joubert. From ultrasoft pseudopotentials to the projector augmented-wave method. *Physical Review B*, 59(3):1758, 1999.
- [40] John P. Perdew, Kieron Burke, and Matthias Ernzerhof. Generalized gradient approximation made simple. *Phys. Rev. Lett.*, 77:3865–3868, Oct 1996.
- [41] Jochen Heyd, Gustavo E. Scuseria, and Matthias Ernzerhof. Hybrid functionals based on a screened coulomb potential. *The Journal of Chemical Physics*, 118(18):8207–8215, 2003.
- [42] D. B. Sinars, S. A. Slutz, M. C. Herrmann, R. D. McBride, M. E. Cuneo, C. A. Jennings, J. P. Chittenden, A. L. Velikovich, K. J. Peterson, R. A. Vesey, C. Nakhleh, E. M. Waisman, B. E. Blue, K. Killebrew, D. Schroen, K. Tomlinson, A. D. Edens, M. R. Lopez, I. C. Smith, J. Shores, V. Bigman, G. R. Bennett, B. W. Ather-ton, M. Savage, W. A. Stygar, G. T. Leifeste, and J. L. Porter. Measurements of magneto-rayleightaylor instability growth during the implosion of initially solid metal liners. *Physics of Plasmas*, 18(5):056301, 2011.
- [43] A. W. DeSilva and J. D. Katsourous. Electrical conductivity of dense copper and aluminum plasmas. *Phys. Rev. E*, 57:5945–5951, May 1998.
- [44] Jean Clérouin, Pierre Noiret, Victor N. Korobenko, and Anatoly D. Rakhel. Direct measurements and ab initio simulations for expanded fluid aluminum in the metal-nonmetal transition range. *Physical Review B*, 78(22):224203, 2008.
- [45] G.R. Gathers. Thermophysical properties of liquid copper and aluminum. *International journal of Thermophysics*, 4(3):209–226, 1983.
- [46] Matthias Leitner, Thomas Leitner, Alexander Schmon, Kirmanj Aziz, and Gernot Pottlacher. Thermophysical properties of liquid aluminum. *Metallurgical and Materials Transactions A*, 48(6):3036–3045, 2017.
- [47] J. P. Perdew and Alex Zunger. Self-interaction correction to density-functional approximations for many-electron systems. *Phys. Rev. B*, 23:5048–5079, May 1981.
- [48] R. Brandt and G. Neuer. Electrical resistivity and thermal conductivity of pure aluminum and aluminum alloys up to and above the melting temperature. *International Journal of Thermophysics*, 28(5):1429–1446, Oct 2007.
- [49] P. D. Desai, H. M. James, and C. Y. Ho. Electrical resistivity of aluminum and manganese. *Journal of Physical and Chemical Reference Data*, 13(4):1131–1172, 1984.
- [50] C. Y. Ho, M. W. Ackerman, K. Y. Wu, T. N. Havill, R. H. Bogaard, R. A. Matula, S. G. Oh, and H. M. James. Electrical resistivity of ten selected binary alloy systems. *Journal of Physical and Chemical Reference Data*, 12(2):183–322, 1983.
- [51] R. O. Simmons and R. W. Balluffi. Measurements of the high-temperature electrical resistance of aluminum: Resistivity of lattice vacancies. *Phys. Rev.*, 117:62–68, Jan 1960.